Natural Wet-Snow Shedding from Overhead Cables

László E. Kollár[1], Ossama Olqma[2] and Masoud Farzaneh[3]

NSERC/Hydro-Québec/UQAC Industrial Chair on Atmospheric Icing of Power Network Equipment (CIGELE) and Canada Research Chair on Atmospheric Icing Engineering of Power Networks (INGIVRE), www.cigele.ca

Université du Québec à Chicoutimi, 555 boulevard de l'Université, Chicoutimi, Québec, Canada G7H 2B1

Abstract

The initiation of wet-snow shedding from overhead cables with negligible sag due to natural processes was modeled experimentally and theoretically. The experiments were carried out in a cold chamber where wet-snow sleeves were prepared on a suspended cable, and then exposed to natural processes leading to snow shedding: air temperature above freezing point, wind effect, and heat radiation. The theoretical model is based on heat balance, and simulates water migration in the cross section at the end of the snow sleeve from the top half toward the bottom half. The model calculates the time history of liquid water content and density of snow in the end section, predicts the deflection of the same section and its shedding when it is completely detached from the cable. The theoretical and experimental results provide the time of snow shedding under different ambient conditions, together with time dependence of liquid water content and density of snow during the time interval modeled.

[1] Corresponding author, Tel.: 1-418-545-5011 / 5606, Fax: 1-418-545-5012, E-mail: laszlo_kollar@uqac.ca
[2] Tel.: 1-418-545-5011 / 2051, Fax: 1-418-545-5032, E-mail: ossamaolq@hotmail.com
[3] Tel.: 1-418-545-5044, Fax: 1-418-545-5032, E-mail: farzaneh@uqac.ca

Keywords: cold-chamber experiments, density, liquid water content, snow shedding, thermodynamic model.

1 Introduction

Wet snow accumulates on overhead transmission lines at air temperatures slightly above freezing point. The accretion may grow under favorable conditions and the accreted snow may persist long time on the cable before shedding occurs at such a point that it endangers the transmission line. The shedding of the accreted wet snow involves a further danger, because it causes unbalanced load on the line. Therefore, predicting the time duration of snow persistence on the cable and understanding the initiation and propagation of wet-snow shedding are particularly important from the point of view of line design. An essential condition for thick accretion to be formed is the presence of liquid water, because this factor is responsible for strong adhesion of wet snow to the cable. However, a further increase of liquid water content (LWC) weakens cohesive and adhesive forces, and leads to snow shedding. Natural processes such as solar radiation, or free or forced convection due to air temperature above freezing point with or without wind effects, cause solid ice particles to melt in wet snow, thus increasing LWC, and eventually resulting in snow shedding naturally under the effect of gravity or wind.

Since wet-snow shedding is rarely observed, it is a challenging problem, and it is not surprising that less research has been carried out in this specific field than on the problems caused by glaze or rime ice. Wet-snow accretion on overhead wires was observed mainly in Japan (Wakahama et al., 1977), in France (Admirat and Lapeyre, 1986; Admirat et al., 1990) and in Iceland (Eliasson and Thorsteins, 2000), although this phenomenon is not limited to these countries. The field observations of Admirat and Lapeyre, 1986 suggest that snow shedding occurs first where axial growth took place. They observed that snow accretion was absent near the towers where cable rotation was reduced due to its high torsional rigidity. Eliasson and Thorsteins, 2000 observed the results of snow shedding, and studied fallen snow samples. Snow shedding under experimental conditions was observed in wind tunnel experiments which were carried out to study wet-snow accretion, but where shedding also occurred in some tests (Sakamoto et al., 1988; Wakahama et al., 1977). The main findings of former experiments and observations on wet-snow shedding are summarized in Sakamoto et al., 2005.

Sophisticated theoretical models for wet-snow shedding have not been developed until now. Admirat et al., 1988 constructed a model for wet-snow accretion including a condition for shedding. They proposed that snow sleeves broke up when the LWC reached 40%. This condition was also applied in the wet-snow accretion models developed in Poots and Skelton, 1994 and in Poots and Skelton, 1995. All of these authors expressed LWC as a percentage of the mass of liquid water divided by the total mass of snow, which will also be done throughout the present paper.

The lack of knowledge on the mechanism of wet-snow shedding was at the source of a research program at CIGELE, where an inexpensive technique was developed by Roberge, 2006 to reproduce wet-snow sleeves in a cold chamber. With that technique, he was able to study wet-snow shedding experimentally, and developed a numerical model to simulate the dynamic effects of snow shedding on the cable. However, he did not vary the atmospheric parameters to examine their influence on snow shedding. The present study aims at determining the effects of natural processes, (i) air temperature above freezing point, (ii) wind, and (iii) solar radiation, on the initiation of wet-snow shedding. In order to achieve this goal, the variation of LWC in the end section of the snow sleeve has to be estimated together with water migration toward the bottom of snow sleeve and with the subsequent deflection of the same section. This is the procedure which precedes the detachment of the end section from the snow sleeve. Former models calculated only the variation of the average LWC in the snow sleeve during the accretion process. Therefore, cold-chamber experiments were conducted in the present research to observe the effects of the parameters mentioned above; furthermore, a two-dimensional (2D) thermodynamic model was developed to simulate the process leading to wet-snow shedding from taut cables under different ambient conditions. Such a model also contributes for line designers to fill the need to predict the time during wet snow persists on the transmission line cable.

2 Experimental Setup and Procedure

This section describes the experimental setup, the procedure for preparing the snow sleeve, the measurement techniques, and the ambient conditions.

2.1 Experimental Setup and Preparation of Snow Sleeve

The experiments were carried out in a cold chamber of the CIGELE laboratories. Snow shedding was simulated from a 5-m-long cable (ALCAN Pigeon ACSR) of diameter

12.75 mm suspended approximately 1 m above the floor. The cable was tensioned so that the sag was reduced to a value so small that its effect was negligible and the cable was considered horizontal.

Wet snow was prepared following the technique proposed by Roberge, 2006. Fresh dry snow available outdoor was collected and spread in the cold chamber where the temperature was kept above freezing point, until the snow reached a LWC value representative for wet snow and became wet enough to stick onto the test cable to form a cylindrical accretion. Admirat et al., 1990 observed the LWC of wet snow between 0 and 14%. Successful snow sleeve preparation required snow sticking firmly enough onto the cable with a LWC of at least 8-10%. So, the goal was to raise the LWC to the range of 10 to 15%. In spite of regular verification of snow quality during this period, the LWC of snow sleeve was sometimes found to exceed 15%, because it is difficult to estimate to what extent the LWC can increase when the snow is compressed to form the snow sleeve. Ideally, the snow density should also be constant at the beginning of each experiment; however, the change in the quality of snow available outdoor caused the variation of initial density in the range of 400-600 kg/m^3.

The snow sleeve was fixed on the cable using a semi-cylindrical mold and a semi-cylindrical hand tool. The mold was placed below the cable and raised until the cable coincided with the axis of the mold. The snow was put in the mold and compressed with the hand tool so that it formed a cylindrical snow sleeve around the cable. Finally, the mold was carefully removed so as not to damage the snow sleeve. Figure 1 shows a resulting snow sleeve with a diameter and length of 9.5 cm and 4.5 m, respectively. The LWC and density were assumed constant initially along the whole length.

2.2 Measurement Techniques

The LWC of snow was measured by the melting calorimetry method. The material used included an adiabatic container whose heat capacity was initially determined, a digital thermocouple to measure temperature, a digital scale to weigh the snow sample, and a measuring glass with scale to measure the volume of water. The procedure begins with measuring 500 ml of hot water (which corresponds to a mass of $m_w = 500$ g), pouring it into the container, and measuring its temperature, T_w. Then, a snow sample of mass, m_s, comparable with that of water is dropped into the hot water quickly. Since the snow is wet, its temperature is assumed $T_s = 0^\circ\mathrm{C}$. The sample melts in about one minute, and then the mixture temperature, T_m, is measured. Once the temperature and mass data are known, the LWC may be calculated from the heat balance of the system including water, wet snow and container. This is a simple calculation which is provided in details in Roberge, 2006.

The precision of this measurement is determined by the precisions of the measuring glass, the scale, the digital thermocouple and the handling procedure when snow is put into container and when some snow or water droplet may fall outside the container. These precisions determine the maximum errors in the parameters which are used in the heat balance of the water-snow-container system (m_w, T_w, m_s, and T_m). In order to find the maximum error in the LWC for the variation of each parameter, the maximum errors were applied in the heat balance for each parameter in the range where they appeared in the measurements ($m_w = 500$ g, $70^\circ\mathrm{C} \le T_w \le 90^\circ\mathrm{C}$, 200 g / 400 g $\le m_s \le 500$ g, and $10^\circ\mathrm{C} \le T_m \le 30^\circ\mathrm{C}$). The two lower limits for m_s are explained by the conditions in the different phases of the experiments. The mass of snow sample was kept close to that of the hot water at the beginning of experiment (lower limit: 400 g). However, it was difficult to take a big sample from the top of accumulation at the end of experiments when most of the snow was turned below the cable at the end of the snow sleeve (see Section 4.1 for details of the snow shedding mechanism). In this phase of the experiments the LWC was quite high (20% or more) even on the top part of the accumulation. Thus, in the error analysis, the lower limit m_s = 200 g was considered for higher values of LWC, whereas the lower limit m_s = 400 g was taken into account when the LWC was lower. Table 1 lists the precisions of the tools and of the handling procedure, the maximum error in each parameter, and the resulting maximum error in the LWC value. The measurement is most sensitive for the variation of mixture temperature, and higher error values arise when snow LWC is low. The worst-case scenario considering errors in all the four parameters means a total error of about 22% of the LWC value.

The density of snow was simply obtained by measuring the mass of snow samples taken with a cylindrical piece of known volume.

2.3 Ambient Conditions

As mentioned in Section 1, the present study examines the effects of three parameters: air temperature, wind speed, and solar radiation. The air temperature of the cold chamber was kept constant during the experiments, and the value of this constant was chosen between 1°C and 5°C. The air velocity was limited to 4 m/s in the cold chamber. The experiments were carried out with three velocities; 4 m/s, 2 m/s, and without wind. It should be noted that in the case of no wind air circulation was still observed in the cold chamber due to cooling, and a speed of about 0.6 m/s was measured. This value was applied in the simulations with no wind. Solar radiation was simulated using three halogen lamps. These lamps were positioned in such a way that the illumination from the middle one covered the entire snow sleeve, whereas both of the two other lamps illuminated half of the snow sleeve (see Fig. 1). Thereby the light from two lamps overlapped along the snow sleeve when all three lamps were switched on, and the illumination of the light was doubled (see Fig. 2). The average illumination along the span was measured to be 450 lx and 900 lx, respectively, when one lamp and three lamps were switched on. Compared to the radiation data measured in Quebec province, Canada, at a latitude of 45° (Atmospheric Environment Service, 1984), the simulated illumination corresponds to the radiation after sunrise or before sunset on a winter day under overcast conditions. The illumination at noon on the same day is 2-3 times greater, and it may be up to 40 times greater at midday on a sunny winter day. However, since the luminous efficiency of the sun is greater than that of halogen lamps, the radiation heat flux from the halogen lamps in the experiments corresponds to that originating from the sun at midday on a cloudy winter day, and it is an order of magnitude less than that originating from the sun at midday on a sunny winter day. The latter condition was not modeled in the experiments due to the power limitation of halogen lamps.

3 Construction of the 2D Thermodynamic Model

This section describes a 2D thermodynamic model which uses heat balance to determine the mass of melted water in the vertical section at the end of the snow sleeve on a horizontal cable, and simulates water migration toward the bottom of the section assuming that no water dripping occurs. The modeled mass transfer leads to deflection of the vertical section, and the process terminates by snow shedding. The computation consists of two main steps. The mass of melted water due to heat convection and heat radiation is calculated in the first step, from which the average LWC and density of the section may be determined. Then, water percolation and the deflection of end section are simulated in the second part, and the variations of LWC and density are calculated for the fractions of the snow sleeve end section which are above and below the line passing through the midpoint of cable. This line, indicated in Fig. 3, will henceforth be called centerline for the sake of simplicity. The second part of the model also predicts to what extent the end section is deflected; when the whole section moved below the centerline, shedding is assumed to have happened and simulation is terminated. The first part of this model and existing snow-accretion models (Grenier et al., 1986; Poots and Skelton, 1994; Poots and Skelton, 1995; Sakamoto, 2000) differ in two main points: (i) the present model assumes that snow accretion has already been ended before the beginning of simulation; (ii) the effect of solar radiation was neglected in accretion models due to cloudy conditions, which is not always the case during shedding; therefore this effect is taken into account in the present model. The second part of this model was not at all considered in accretion models, but it is essential for the understanding of the shedding mechanism.

3.1 Heat Balance of Wet Snow Sleeve

The heat balance has been applied in several models of snow accumulation (Grenier et al., 1986; Poots and Skelton, 1994; Poots and Skelton, 1995; Sakamoto, 2000). The present model, assuming that wet-snow accumulation has already been terminated, simulates thermodynamic processes occurring in the snow sleeve until it sheds. The terms which appear in the heat balance in the mentioned models together with heat radiation are considered here, without assuming snow precipitation:

$$Q_f = Q_c + Q_e + Q_r + Q_J \tag{1}$$

where Q_f (W) is the latent heat required to melt the snow, Q_c (W) is the convective heat, Q_e (W) is the heat transfer due to evaporation or condensation, Q_r (W) is the heat gained from radiation, and Q_J (W) is the heat generated by the current.

Since no accumulation is assumed during the process simulated, the heat required to melt the snow is simply calculated as follows:

$$Q_f = L_f \frac{\mathrm{d}M_f}{\mathrm{d}t} \tag{2}$$

where M_f (kg) is the mass of melted water within the snow matrix, t (s) is time, and L_f (J/kg) is the latent heat of fusion.

The convective heat transfer between the ambient air and the snow layer is expressed by

$$Q_c = hA_c\left(T_a - T_s\right) \tag{3}$$

with $h\left(\mathrm{W}/\left(\mathrm{m}^2 \times \mathrm{K}\right)\right)$ standing for heat transfer coefficient, A_c (m^2) denoting the circumferential surface area of exchange, whereas T_a ($^\circ\mathrm{C}$) and T_s ($^\circ\mathrm{C}$) denote temperature of air and snow surface, respectively. The heat transfer coefficient is related to the Nusselt number, Nu, as follows:

$$h = \frac{k_a \mathrm{Nu}}{D} \tag{4}$$

where k_a $\left(\mathrm{W}/\left(\mathrm{m} \times \mathrm{K}\right)\right)$ is the thermal conductivity of air, and D (m) is the diameter of accreted snow. For free convection, the Nusselt number is related to the Grashof number, $\mathrm{Gr} = g\beta_a\left(T_a - T_s\right)D^3/\nu_a^2$, and the Prandtl number, $\mathrm{Pr} = \mu_a c_p / k_a$, with the parameters, g ($\mathrm{m/s}^2$), gravitational constant, β_a (1/K), thermal expansion coefficient of air, ν_a (m^2/s) and μ_a $\left(\mathrm{kg}/\left(\mathrm{m} \times \mathrm{s}\right)\right)$, kinematic and dynamic viscosity of air, respectively, and c_p $\left(\mathrm{J}/\left(\mathrm{kg} \times \mathrm{K}\right)\right)$, specific heat of air at constant pressure. The following correlation was proposed by Bird et al., 1960 to calculate Nusselt number for free convection when $\mathrm{GrPr} > 10^4$:

$$\mathrm{Nu}_{fr} = 0.525\left(\mathrm{GrPr}\right)^{1/4} \tag{5}$$

In case of forced convection, the Nusselt number depends on the Reynolds number, $\mathrm{Re} = \rho_a U_a D / \mu_a$, where ρ_a ($\mathrm{kg/m}^3$) is air density, and U_a (m/s) is wind speed. The correlation proposed by Makkonen, 1984 in the range of $7 \times 10^4 < \mathrm{Re} < 9 \times 10^5$ was applied in this model:

$$\mathrm{Nu}_{fo} = 0.032\,\mathrm{Re}^{0.85} \tag{6}$$

The heat transfer due to evaporation of liquid water or condensation of water vapor is obtained from the formula:

$$Q_e = M_{w,a}\left(\frac{\mathrm{Pr}}{\mathrm{Sc}}\right)^{0.63}\frac{L_v}{c_p}hA_c\frac{\Delta e_w}{p} \tag{7}$$

where $M_{w,a} = 0.622$ is the ratio of the molar weights of water vapor and air, $\mathrm{Sc} = \nu_a / D_{w,a}$ is the Schmidt number, $D_{w,a}$ ($\mathrm{m^2/s}$) is the diffusion coefficient of water vapor in air, L_v (J/kg) is the latent heat of vaporization, $p = 101325\ \mathrm{Pa}$ is the atmospheric pressure, and $\Delta e_w = \varphi e_w(T_a) - e_w(T_s)$ is the difference between vapor pressure in the air and at the snow surface with $e_w(T)$ (Pa) and φ, which denote saturation vapor pressure at temperature T and relative humidity of air, respectively. The relative humidity of air was assumed constant in the experiments: $\varphi = 0.8$.

The heat gained from radiation is the sum of short-wave radiation originating from the halogen lamps and long-wave radiation between the snow and the chamber walls. Both short-wave and long-wave radiations are also present in natural processes, originating from the Sun and the atmosphere, respectively. The heat transfer due to radiation may be calculated from the following formula:

$$Q_r = (1-\alpha)I_r A_r + \varepsilon\sigma_R\left(T_a^4 - T_s^4\right)A_c \tag{8}$$

The intensity, I_r $\left(\mathrm{W/m^2}\right)$, is obtained from the value measured in lx divided by the product of 683 lm/W and the luminous efficiency of the halogen lamp. The halogen lamp operates at a filament temperature of around $3000\ \mathrm{K}$, with luminous efficiency taken to be 3.5% according to Planck's law. The radiated surface, A_r ($\mathrm{m^2}$), is the projection of the sleeve surface in the plane perpendicular to radiation. The albedo of wet snow, α, is taken to be 0.6 (Male and Grey, 1981), whereas the emissivity of snow, ε, is equal to 0.98 (Kondratyev, 1969). The $\sigma_R = 5.57 \times 10^{-8}$ W/$\left(\mathrm{m}^2 \times \mathrm{K}^4\right)$ is the Stefan-Boltzmann constant, and the temperature of chamber walls is assumed to be equal to the air temperature, T_a ($^\circ$C). Although heat radiation is neglected in snow accumulation models, because snow usually accumulates under overcast conditions, the present model takes it into account, which makes it possible to evaluate the effect of solar radiation on snow shedding.

The heat due to Joule effect is produced by the current carried in the cable, and also depends on the electric resistance of the cable. As the effect of electric current is the subject of a parallel project, this term is left out of the present model.

3.2 Water Movement through Snow and Deflection of End Section

LWC and density are assumed to be constant initially in the cross section of the snow sleeve. Then, once the water distribution in snow is in funicular mode, the liquid water begins to migrate from the top toward the bottom. If, for the sake of simplicity, the capillary influence on water flow is ignored, then the flow occurs under the effect of gravity, and can thus be described by the simplified form of Darcy's law (Colbeck, 1972):

$$u_w = k_w \frac{\rho_w g}{\mu_w} \tag{10}$$

where u_w (m/s) is the volume flux of water, k_w (m^2) is the permeability to the water phase, ρ_w ($\mathrm{kg/m^3}$) is the density of water, and μ_w $(\mathrm{kg}/(\mathrm{m}\times\mathrm{s}))$ is the dynamic viscosity of water. The permeability, k_w, is related to the porosity, ϕ, and water saturation, S_w. If the water film is not continuous from ice grain to ice grain, then the permeability is 0 and no water flow occurs. This fact suggests to relate permeability to another parameter, $S = (S_w - S_{wi})/(1 - S_{wi})$, where S_{wi} is the value of saturation when the water film becomes continuous, called irreducible water saturation, and $S = 0$ if $S_w < S_{wi}$. This saturation corresponds to the transition between the pendular and funicular regimes of liquid distribution, which occurs around 14% (Denoth, 1980). Then, permeability can be obtained by the following equation:

$$k_w = a\exp(b\phi)S^2 \tag{11}$$

where a(m^2) and b are constants. The value derived by Colbeck, 1972 for a, 6.25×10^{-14} m^2, was applied in the model. The value of the other constant, $b = 8$, was chosen in correspondence with experimental observations. The porosity, ϕ, and saturation, S_w, are related to the LWC, Λ, and density of snow, ρ ($\mathrm{kg/m^3}$) as follows (Denoth, 1980):

$$\phi = 1 - \rho(1 - \Lambda)/\rho_i \tag{12}$$

$$S_w = (\rho/\rho_w)\Lambda/\phi \tag{13}$$

with ρ_i ($\mathrm{kg/m^3}$) denoting the density of ice.

The development of cavities below the cable and the deflection of end section are modeled as follows. Liquid water percolates toward the inferior parts of the snow matrix under the effect of gravity. Thus, water flows away from the snow which is located directly below the cable, but the cable prevents water to flow here from the upper parts of snow. Consequently, a cavity starts enlarging below the cable at the end of the snow sleeve where cohesion in the snow is weaker. The flow of water migrating away from the lower limit of the cavity in the end section is the product of the volume flux of water, u_w, and the length of the arc limiting the cavity from the bottom. This arc length is equal to the half of the circumference of the cable. The flow of this migrating water in time, *t*, creates a cavity with an area which is the product of the cable diameter, *d*, and the deflection of end section in the same time, *y*. This equality provides the length, *y*, as a function of time (step b in Fig. 3).

3.3 Procedure of Computation

Since the model is two dimensional, all the calculations concern a unit length of cylinder with the assumptions being valid in the end section of the snow sleeve. Thus, the unit length practically means an infinitesimal length at the end of snow sleeve. First, the mass of melted water in unit time in this section is determined from heat balance. Knowing the ambient conditions, the initial mass and initial LWC, then the average LWC in the section may easily be calculated at any time. Second, the deflection of the end section is obtained in each time step as explained in the previous subsection, and the LWC and density of the snow above and below the centerline is determined. In order to achieve this goal, each time step during the process in the second part is divided into three sub-steps numerically as shown in Fig. 3. In the first sub-step (step (a) in Fig. 3), the snow sleeve shrinks, with consequent increase in density, so that a new radius, $R(i+1)$, is calculated due to this change and accordingly with the assumption which is based on experimental observations: the increase in density is proportional to the increase in LWC. In the second sub-step (step (b) in Fig. 3), the size of cavity increases, and correspondingly, the deflection of end section increases to $y(i+1)$. The area, $\Delta A(i)$, which was in the top part of the snow sleeve before the *i*th time step, moves to the bottom part, because it is located below the centerline of the (*i*+1)st time step. In the third sub-step (step (c) in Fig. 3), water flows downward inside the snow matrix. The quantity of water which passes by the centerline during a time step Δt, $\Delta M_w(i)$, is calculated after applying another experimentally established assumption: the quantity of this water is 50% of the water which melted during the same time, Δt. Consequently, the mass of snow above the centerline after the *i*th time step, $M_1(i+1)$, is equal to this mass in the preceding time step, $M_1(i)$, minus the mass of snow in the area $\Delta A(i)$, minus the quantity of water which passes the centerline in the *i*th time step, $\Delta M_w(i)$. Since the density of snow is assumed to be the same in the entire top part of the section, the ratio of masses is equal to the ratio of areas; therefore

$$M_1(i+1) = M_1(i) - \frac{\Delta A(i)}{A_1(i)} M_1(i) - \Delta M_w(i) \tag{14}$$

Since water dripping is not considered, and the evaporated mass is negligible, the total mass, M, is maintained constant, and the mass of snow below the centerline after the *i*th time step is obtained from:

$$M_2(i+1) = M - M_1(i+1) \tag{15}$$

The indices 1 and 2 refer to the parts above and below the centerline, respectively. The mass of water above the centerline after the *i*th time step, $M_{1w}(i+1)$, is equal to the mass after the preceding time step, $M_{1w}(i)$, plus the mass of water melted in the *i*th time step in the snow which is above the centerline, minus the mass of water in the area $\Delta A(i)$, minus the quantity of water which passes the centerline in the *i*th time step, $\Delta M_w(i)$:

$$M_{1w}(i+1) = M_{1w}(i) + \frac{A_1(i)}{A(i)} M_f(i) - \frac{\Delta A(i)}{A_1(i)} M_{1w}(i) - \Delta M_w(i) \tag{16}$$

where *A* is the total area of the cross section. The mass of water below the centerline after the *i*th time step, $M_{2w}(i+1)$, is similarly obtained from:

$$M_{2w}(i+1) = M_{2w}(i) + \left(1 - \frac{A_1(i)}{A(i)}\right) M_f(i) + \frac{\Delta A(i)}{A_1(i)} M_{1w}(i) + \Delta M_w(i) \tag{17}$$

Once the mass of snow, the mass of water and the area above and below the centerline are known, the LWC and density may easily be calculated in both parts of the end section of the snow sleeve. The procedure is repeated until the entire end section turns below the centerline, when shedding is assumed and computation is terminated. The values of the parameters describing the physical properties of air, water and ice are listed in Table 2.

4 Results and Discussion

This section presents the observed shedding mechanism as well as experimental and computational results of modeling snow shedding.

4.1 Shedding Mechanism

A typical example of the deformation of the end section of a snow sleeve during the shedding mechanism is shown in Fig. 4. Initially, the snow sleeve is homogeneous; its circumference forms a circle concentric with the cable (Fig. 4a). As time goes on, water migrates toward the bottom of the sleeve, and the bottom part of the sleeve becomes more and more transparent. Simultaneously, the end section begins to turn down, and a zone of cavity appears below the cable (Figs. 4b and 4c). However, the cross section remains approximately circular during this deformation. Further down in the process, the entire end section turns below the cable, and water droplets may start falling at the tip of the section (Fig. 4d). This step in most of the experiments is very short as compared to the whole duration of the process, ending with the shedding of a 20 to 30-cm-long snow chunk. Nevertheless, there were a few experiments when the cohesion in the snow delayed shedding. In these cases, the LWC increased linearly in time, and then remained approximately constant during a relatively longer period during which water dripping was already observed. Since this time was short in the majority of experiments, and water dripping was not observed until this very last part of the shedding mechanism, the theoretical model stops when the entire end section turns below the cable, so that water dripping is not considered in the model.

4.2 Experimental Results

Experiments were carried out under several different ambient conditions as explained in Section 2. This subsection compares the effects of the three ambient parameters examined: (i) temperature, (ii) wind speed, (iii) heat radiation. During the experiments, one end of the snow sleeve is never touched, whereas the LWC and density are measured from time to time at the other end of the sleeve. At the end of each experiment, these properties are measured from the shed pieces of snow. Shedding time including the time of the whole process till actual shedding is also recorded.

Table 3 presents a summary of the experimental results, including the adjusted ambient conditions, and the measured parameters which are the initial and final LWC and densities, the shedding time, and the average slope describing the increase in LWC at the end section in time (slope of the linear fit on measured data points such as the lines shown in Figs 5-7). Density measurement requires a large enough unbroken piece of snow which was not always available after shedding; therefore the time in parentheses appearing below most of the final density data indicates when the last density measurement took place. According to these results, the lowest LWC values of shedding snow were measured around 35%, and they might go up to about 55%. It should be noted that the highest measured values of LWC may overestimate the real LWC, because the snow was slushy and the snow sample melted quickly even on the plate where it fell and where it was carried for measuring its LWC. The 40% estimate applied in previous models (Admirat et al., 1988; Poots and Skelton, 1994; Poots and Skelton, 1995) falls in this range, but the width of this range is considerably greater than a few % which could be attributed to measurement error. However, the 40% estimate used in those models is valid during the accumulation process. So, the process simulated with the 40% estimate is different from the one considered here. The interval of measured values for final density is 600-870 $\mathrm{kg/m^3}$. The results of an experiment which was carried out at an air temperature of $1\,^\circ\mathrm{C}$ do not appear in Table 3, because that experiment lasted 23 h, including the night period when conditions were not controlled, so that the obtained results were rejected.

Figure 5 reveals how increasing air temperature accelerates the shedding process by showing time histories of LWC with air temperature as parameter. The shedding time is reduced significantly, more precisely by a factor of approximately 2.7, when temperature is increased from $2^\circ C$ to $5^\circ C$. The slope of the line representing the increase in LWC also increases by a factor of 2.3 – 2.5.

The effect of wind speed on snow shedding may be observed in Fig. 6. A small increase in velocity, from 0.6 to 4 m/s, reduces shedding time to the one third of its value. It should be kept in mind, however, that the initial LWC was considerably higher for 4 m/s than the desired range of 10-15%, which must have contributed to the early shedding. Nevertheless, the significant effect of air velocity is not an exaggeration, because the slope of increase in LWC also changed by a factor of around 3 when the velocity was increased from 0.6 to 4 m/s.

Figure 7 presents time histories of LWC with the third parameter under investigation, i.e. heat radiation. The application of halogen lamps influences the shedding process to a significantly less extent than an increase in air temperature or wind speed. The shedding time and the slope of the increase in LWC are almost identical for intensities of 0 lx and 450 lx, whereas the slope is greater by a factor of approximately 1.3 for 900 lx. The only considerable difference observed is the diminution in shedding time for the 900 lx intensity. This change may possibly be explained by an undesirable effect, such as the different quality of snow available outdoor preceding different experiments or a crack produced during the preparation of the sleeve.

4.3 Comparison of Experimental Observations and Computer Simulations

The theoretical model described in Section 3 was applied for several different conditions, and the obtained simulation results were compared to experimental observations. Since the duration of the experiments took several hours, the time step of calculation was chosen to be one minute. Figure 8 shows time histories of LWC as calculated in the entire end section as well as in the top and bottom half of the same section. Measured values of LWC of the snow sleeve are also plotted in this figure. In some of the experiments two samples were taken at each measurement, one from the top and one from the bottom half of the snow sleeve (see Figs. 8c and 8d). The four diagrams in Fig. 8 were chosen to help compare the effects of changing each parameter when the other parameters are not varied. At the beginning of most of the experiments the LWC increases by the same extent everywhere in the snow sleeve, because ice grains start melting, but water percolation is not occurring yet (curves for “simulation, bottom” and “simulation, top” coincide at the beginning in Figs. 8a,c,d and 9). As LWC increases, the water distribution in snow is in funicular mode, water movement toward the bottom of the snow sleeve begins, and the end section starts turning down. Consequently, the LWC increase in the top part slows down, and, at the same time, it accelerates in the bottom part (curves for “simulation, bottom” and “simulation, top” have different slopes and diverge in Figs. 8 and 9). At the end of the experiment, the top part disappears and the LWC in the bottom part approaches the average LWC of the entire section, because the whole section is deflected below the cable (“simulation, bottom” curve approaches “simulation” curve in Figs. 8 and 9). It should be noticed that water distribution was in funicular mode even at the beginning of the experiment whose simulation results are shown in Fig. 8b. Therefore, the increase in LWC in the top differs from that in the bottom part from the very beginning. Variations in density for the entire section, in the top and the bottom parts are plotted and compared to experimental results for one ambient condition in Fig. 9, where similar tendencies may be observed as for LWC. The difference is that the density does not approach 0 as the LWC does when the mass of snow on the top reduces significantly. In this moment, even a very small amount of water causes a slight increase in the density, since the volume also becomes very small. Although this increase in the density is just a few percent, it was not evaluated as realistic; therefore the density calculated on the top is not presented after this moment. Although the discrepancy between the measured and simulated values is changeable, the increasing tendencies, i.e. the slopes of the curves and the shedding times, are predicted satisfactorily by the model. In the few cases when shedding was delayed by stronger cohesion in the snow, the model is applicable to predict the increase of LWC; however, it fails to estimate shedding time, because the period with approximately constant LWC and with water dripping is not considered. This problem appears to be a challenge in future research. The reader is referred to Olqma, 2009 for further results and details.

Simulation results are compared to former experimental observations in Fig. 10. The time history of LWC is presented in this figure for the conditions of an experiment carried out by Roberge, 2006. The model provides an acceptable estimation for both of the increase of LWC and the shedding time. The slope of increase of LWC is calculated as 4.4 % / h, and measured as 5.1 % / h; whereas the computed and experimentally obtained shedding times are 7h 27min and 6h 38min, respectively. Both discrepancies are within 15%. It should be noted, that the calculated curves in Fig. 10 do not coincide with those in Fig. 8a, because the initial conditions (LWC, density) were different.

The evaluation of different terms in the heat balance makes possible a qualitative comparison between the influences of different heat sources. Table 4 shows the contribution of each heat source when air temperature, wind velocity, and intensity of short-wave radiation are varied. Since the air speed was practically 0.6 m/s in the cases with “no wind” (see Section 2.3), heat flux data are also presented for this velocity. This comparison confirms what was obtained in the experiments: the influence of increasing temperature and wind velocity dominates over the influence of heat radiation. It should be noted, however, that under sunny conditions the heat transfer rate due to short-wave radiation may reach, or even exceed, that due to convection under calm conditions.

5 Conclusions and Recommendations

Wet-snow shedding from a suspended cable with negligible sag under natural conditions has been studied experimentally, and a thermodynamic model has been developed to simulate the variation of LWC and density at the end section of the snow sleeve until shedding. The effects of three parameters were considered: air temperature, wind velocity and solar radiation. Experimental results show that snow shedding under natural conditions begins at the end of the snow sleeve. At the beginning of the shedding process LWC increases in the entire end section, then water starts migrating toward the bottom of sleeve. Eventually, the end section becomes more and more deflected until the snow sheds, when external forces exceed adhesive and cohesive forces. Increasing air temperature and wind velocity accelerate this process significantly. The effect of solar radiation is less important when the sky is cloudy though it becomes considerable under sunny conditions. The theoretical model predicts satisfactorily the rate of increase of LWC and the shedding time. The final LWC and final density of the snow when it sheds vary within a considerably wide range.

The process of snow shedding implies a number of further questions which are out of the scope of the present study, but should be addressed in future research. Some of these topics are as follows: modeling snow shedding from a current-carrying conductor; studying the snow shedding process from a sagged cable; finding the dependence of final LWC and final density on the initial snow characteristics; extending the thermodynamic model to 3D; and defining a shedding condition in terms of external and adhesive forces, which may help to predict rupture in the model of a 3D snow sleeve.

Acknowledgments

This work was carried out within the framework of the NSERC/Hydro-Québec/UQAC Industrial Chair on Atmospheric Icing of Power Network Equipment (CIGELE) and the Canada Research Chair on Engineering of Power Network Atmospheric Icing (INGIVRE) at the Université du Québec à Chicoutimi. The authors would like to thank the CIGELE partners (Hydro-Québec, Hydro One, Électricité de France, Alcan Cable, K-Line Insulators, CQRDA and FUQAC) whose financial support made this research possible.

References

Admirat, P. and Lapeyre, J.L., 1986. Observation d'accumulation de neige collante à la station de Bagnères de Luchon les 6, 7 avril 1986 - Effet préventif des contrepoids antitorsion, EDF-DER HM/72-5535.

Admirat, P., Lapeyre, J.L. and Dalle, B., 1990. Synthesis of Filed Observations and Practical Results of the 1983-1990 "Wet-Snow" Programme of Electricité de France, Proc. of 5th International Workshop on Atmospheric Icing of Structures, Tokyo, Japan, pp. B6-2-(1) - B6-2-(5).

Admirat, P., Maccagnan, M. and Goncourt, B.D., 1988. Influence of Joule effect and of climatic conditions on liquid water content of snow accreted on conductors, Proc. of 4th International Workshop on Atmospheric Icing of Structures, Paris, France.

Atmospheric Environment Service, 1984. Monthly Radiation Summary, 25. Environment Canada.

Bird, R.B., Stewart, W.E. and Lightfoot, E.N., 1960. Transport Phenomena. John Wiley & Sons Inc., New York, NY, USA.

Colbeck, S.C., 1972. A Theory of Water Percolation in Snow. Journal of Glaciology, 11(63): 369-385.

Denoth, A., 1980. The Pendular-Funicular Liquid Transition in Snow. Journal of Glaciology, 25(91): 93-97.

Eliasson, A.J. and Thorsteins, E., 2000. Field Measurements of Wet Snow Icing Accumulation, Proc. of 9th International Workshop on Atmospheric Icing of Structures, Chester, England.

Grenier, J.C., Admirat, P. and Maccagnan, M., 1986. Theoretical Study of the Heat Balance during the Growth of Wet Snow Sleeves on Electrical Conductors, Proc. of 3rd International Workshop on Atmospheric Icing of Structures, Vancouver, BC, Canada, pp. 125-129.

Kondratyev, K.Y., 1969. Radiation in the Atmosphere. Academic Press, New York, NY.

Makkonen, L., 1984. Modeling of Ice Accretion on Wires. Journal of Climate and Applied Meteorology, 23(6): 929-938.

Male, D.H. and Grey, D.M., 1981. Snowcover Ablation and Runoff. In: D.M. Grey and D.H. Male (Editors), Handbook of Snow. Pergamon Press, Toronto, ON.

Olqma, O., 2009. Critères de déclenchement du délestage de la neige collante de câbles aériens (Criteria for Initiation of Snow Shedding from Overhead Cables, in French), University of Quebec at Chicoutimi, Chicoutimi, QC, submitted.

Poots, G. and Skelton, P.L.I., 1994. Simple models for wet-snow accretion on transmission lines: snow load and liquid water content. International Journal of Heat and Fluid Flow, 15(5): 411-417.

Poots, G. and Skelton, P.L.I., 1995. Thermodynamic models of wet-snow accretion: axial growth and liquid water content on a fixed conductor. International Journal of Heat and Fluid Flow, 16(1): 43-49.

Roberge, M., 2006. A Study of Wet Snow Shedding from an Overhead Cable. M.Sc. Thesis, McGill University, Montreal, QC.

Sakamoto, Y., 2000. Snow accretion on overhead wires. Phil. Trans. R. Soc. Lond. A, 358: 2941-2970.

Sakamoto, Y., Admirat, P., Lapeyre, J.L. and Maccagnan, M., 1988. Thermodynamic simulation of wet snow accretion under wind-tunnel conditions, Proc. of 4th International Workshop on Atmospheric Icing of Structures, Paris, France, pp. Paper A6.6.

Sakamoto, Y., Tachizaki, S. and Sudo, N., 2005. Snow Accretion on Overhead Wires, Proc. of 11th International Workshop on Atmospheric Icing of Structures, Montreal, QC, Canada, pp. 3-9.

Wakahama, G., Kuroiwa, D. and Goto, K., 1977. Snow Accretion on Electric Wires and its Prevention. Journal of Glaciology, 19(81): 479-487.

Tables

Source of error	Precision	Parameter affected by source of error	Max error in parameter	Max error in LWC value
Scale on measuring glass	± 0.5 ml	Mass of water, m_w	± 0.5 g	$\pm 2\%$
Digital scale	± 0.01 g	Mass of snow sample, m_s	± 0.51 g	$\pm 1\%$
Handling procedure	± 0.5 g			
Digital thermocouple	$\pm 0.5^{\circ}$C	Temperature of hot water, T_w	$\pm 0.5^{\circ}$C	$\pm 6\%$
		Temperature of mixture, T_m	$\pm 0.5^{\circ}$C	$\pm 13\%$

Table 1: Maximum error in the LWC measurement

Parameter	Symbol	Unit	Value
Specific heat of air	c_p	$\mathrm{J/(kg \times K)}$	1006
Diffusion coefficient of water vapor in air	$D_{w,a}$	$\mathrm{m^2/s}$	2.1×10^{-5}
Thermal conductivity of air	k_a	$\mathrm{W/(m \times K)}$	2.42×10^{-2}
Latent heat of fusion	L_f	J/kg	3.35×10^{5}
Latent heat of vaporization	L_v	J/kg	2.5×10^{6}
Thermal expansion coefficient of air	β_a	1/K	$1/((T_a + T_s)/2)$
Dynamic viscosity of air	μ_a	$\mathrm{kg/(m \times s)}$	1.73×10^{-5}
Dynamic viscosity of water	μ_w	$\mathrm{kg/(m \times s)}$	1.79×10^{-3}
Kinematic viscosity of air	ν_a	$\mathrm{m^2/s}$	1.34×10^{-5}
Density of air	ρ_a	$\mathrm{kg/m^3}$	1.28
Density of water	ρ_w	$\mathrm{kg/m^3}$	1000
Density of ice	ρ_i	$\mathrm{kg/m^3}$	917

Table 2: Physical parameters describing air, water and ice (temperature dependent parameters are considered at $3\,^\circ\mathrm{C}$)

T_a (°C)	U_a (m/s)	Illumi-nation (lx)	Initial LWC (%)	Initial density (kg/m^3)	Final LWC (%)	Final density (kg/m^3)	Shedding time (h:min)	Average slope (% / h)
2	0*	0	29.4	550	45.8	870 (12:00)**	13:00	1.1
3	0	0	12.2	440	40.2	510 (4:00)	7:00	4.8
5	0	0	12.5	460	43.1	730 (6:00)	6:40	4.4
2	2	0	10.0	670	42.5	870	7:00	3.4
3	2	0	15.2	640	50.0	800 (5:00)	6:45	5.9
5	2	0	20.2	540	59.6	850 (3:00)	3:40	10.0
2	4	0	14.2	500	56.8	790 (5:00)	5:30	5.7
3	4	0	12.3	580	46.8	-	3:15	10.1
5	4	0	23.2	580	49.6	640 (1:00)	2:00	13.3
2	0	450	10.0	420	41.9	600	3:25	8.2
3	0	450	8.5	420	43.2	590 (6:10)	7:45	4.5
5	0	450	24.6	590	49.5	0.64	3:10	7.9
2	0	900	9.7	540	44.8	770 (4:00)	7:40	4.6
3	0	900	11.8	520	36.3	0.71	4:00	6.1
5	0	900	16.0	520	47.5	680 (1:00)	2:50	11.2

Table 3: Summary of experimental results; * - 0 means “no wind” case, but a velocity of about 0.6 m/s of the circulating air was still measured; ** - time in parentheses below final density data indicates time of last density measurement if it took place earlier than the end of experiment

Convective heat flux, q_c ($\mathrm{W/m^2}$)			
	$T_a = 2^{\circ}\mathrm{C}$	$T_a = 3^{\circ}\mathrm{C}$	$T_a = 5^{\circ}\mathrm{C}$
$U_a = 0$ m/s	6	9	15
$U_a = 0.6$ m/s	21	31	52
$U_a = 2$ m/s	56	84	140
$U_a = 4$ m/s	100	149	249
$U_a = 10$ m/s	213	314	533

(a)

Heat flux due to short-wave radiation, $q_{r,s}$			
condition	exp, 450 lx	exp, 900 lx	sunny winter day
$q_{r,s}$ ($\mathrm{W/m^2}$)	7.5	15	167*

(b)

Heat flux due to long-wave radiation, $q_{r,l}$			
T_a $\left(^{\circ}\mathrm{C}\right)$	2	3	5
$q_{r,l}$ ($\mathrm{W/m^2}$)	9	14	23

(c)

Heat flux due to evaporation / condensation, q_e ($\mathrm{W/m^2}$)			
	$T_a = 2^{\circ}\mathrm{C}$	$T_a = 3^{\circ}\mathrm{C}$	$T_a = 5^{\circ}\mathrm{C}$
$U_a = 0$ m/s	-2.3	-0.2	4.5
$U_a = 0.6$ m/s	-8.0	-0.7	15
$U_a = 2$ m/s	-22	-1.9	42
$U_a = 4$ m/s	-39	-3.4	74
$U_a = 10$ m/s	-83	-7.3	159

(d)

Table 4: Heat fluxes under different ambient conditions, (a) heat convection, (b) heat due to short-wave radiation considering a snow albedo of 0.6, (c) heat due to long-wave radiation, (d) heat due to evaporation / condensation for a relative humidity of 0.8; * -

value corresponds to 1.5 $\mathrm{MJ}/\left(\mathrm{m}^2 \times \mathrm{h}\right)$ which is measured at midday on sunny winter days (Atmospheric Environment Service, 1984)

Figure Captions

Fig. 1: Snow sleeve on the suspended cable at the beginning of an experience using one lamp to simulate heat radiation

Fig. 2: Illumination of the snow sleeve by the halogen lamps

Fig. 3: Three numerical sub-steps in the *i*th time step to calculate deflection of end section as well as LWC and density above and below centerline

Fig. 4: Evolution of deflection of snow sleeve during the shedding mechanism ($T_a = 5\,^{\circ}\mathrm{C}$, $U_a = 2$ m/s, no radiation), (a) t = 0h; (b) t = 1h; (c) t = 2h; (d) t = 3h

Fig. 5: Time histories of LWC until snow shedding with air temperature as parameter; (a) $U_a = 4$ m/s, no radiation; (b) $I_r = 900$ lx, no wind

Fig. 6: Time histories of LWC until snow shedding with wind speed as parameter, $T_a = 5\,^{\circ}\mathrm{C}$, no radiation

Fig. 7: Time histories of LWC until snow shedding with heat radiation as parameter, $T_a = 3\,^{\circ}\mathrm{C}$, no wind

Fig. 8: Measured (experiment) and calculated (simulation) LWC time histories, (a) $T_a = 3^{\circ}\mathrm{C}$, no wind, no radiation, (b) $T_a = 3^{\circ}\mathrm{C}$, $U_a = 4$ m/s, no radiation, (c) $T_a = 2^{\circ}\mathrm{C}$, $U_a = 4$ m/s, no radiation, (d) $T_a = 3^{\circ}\mathrm{C}$, no wind, $I_r = 450$ lx

Fig. 9: Measured (experiment) and calculated (simulation) density time histories for $T_a = 3^{\circ}\mathrm{C}$, no wind, no radiation

Fig. 10: LWC time histories as measured by Roberge, 2006 (experiment) and calculated by the present model (simulation) for $T_a = 3^{\circ}\mathrm{C}$, no wind, no radiation

Fig. 1: Snow sleeve on the suspended cable at the beginning of an experience using one lamp to simulate heat radiation

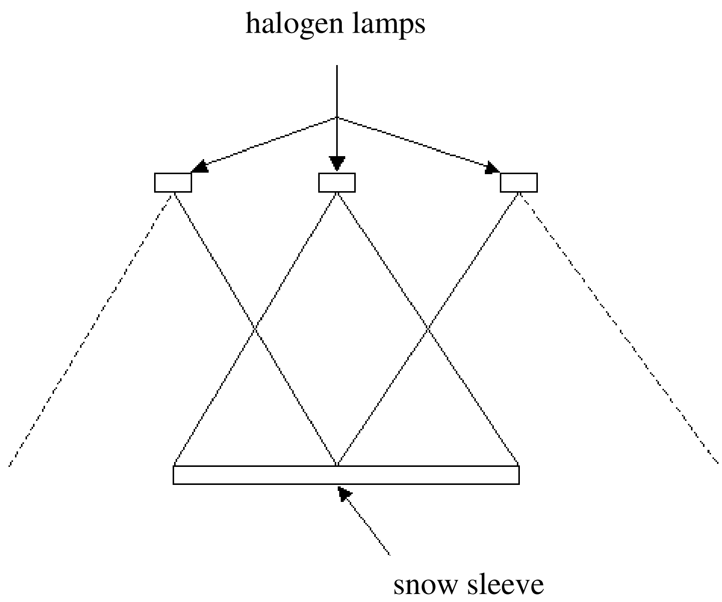

Fig. 2: Illumination of the snow sleeve by the halogen lamps

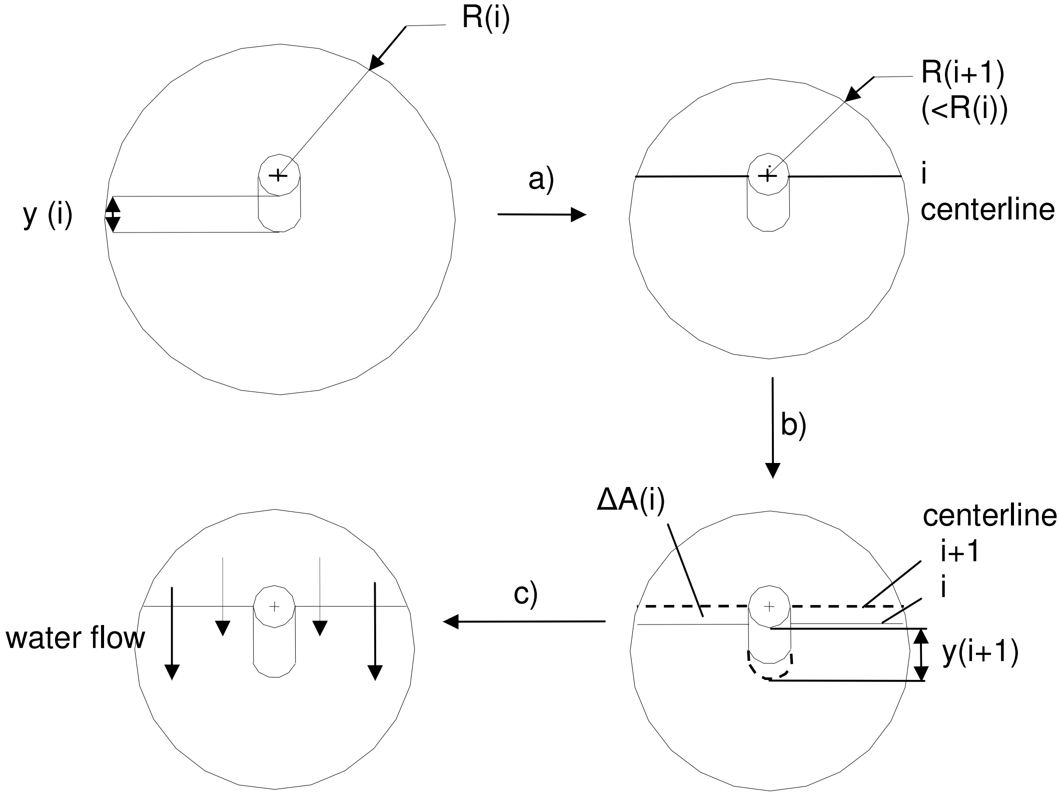

Fig. 3: Three numerical sub-steps in the *i*th time step to calculate deflection of end section as well as LWC and density above and below centerline

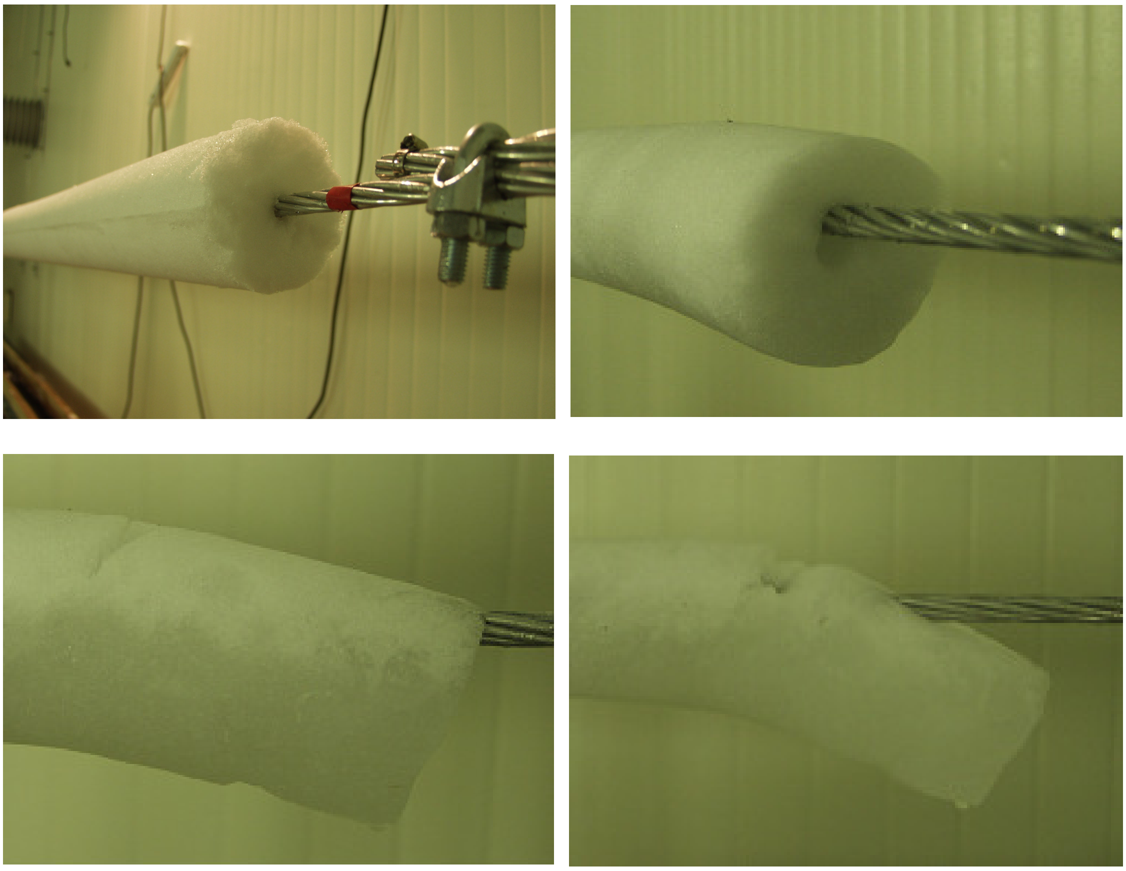

Fig. 4: Evolution of deflection of snow sleeve during the shedding mechanism ($T_a = 5\,^\circ\mathrm{C}$, $U_a = 2$ m/s, no radiation), (a) t = 0h; (b) t = 1h; (c) t = 2h; (d) t = 3h

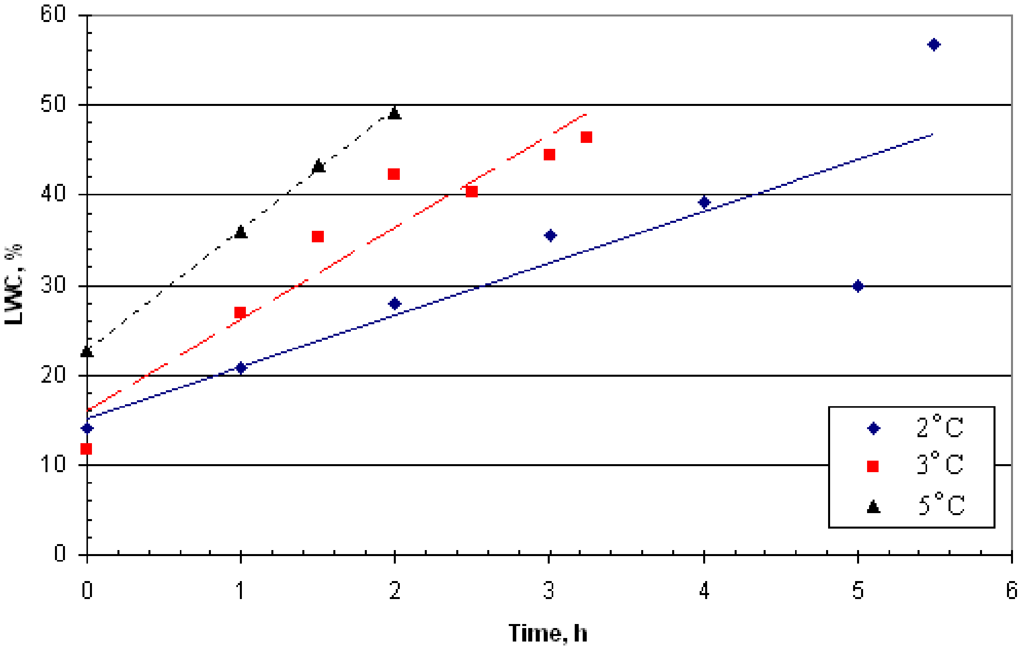

(a)

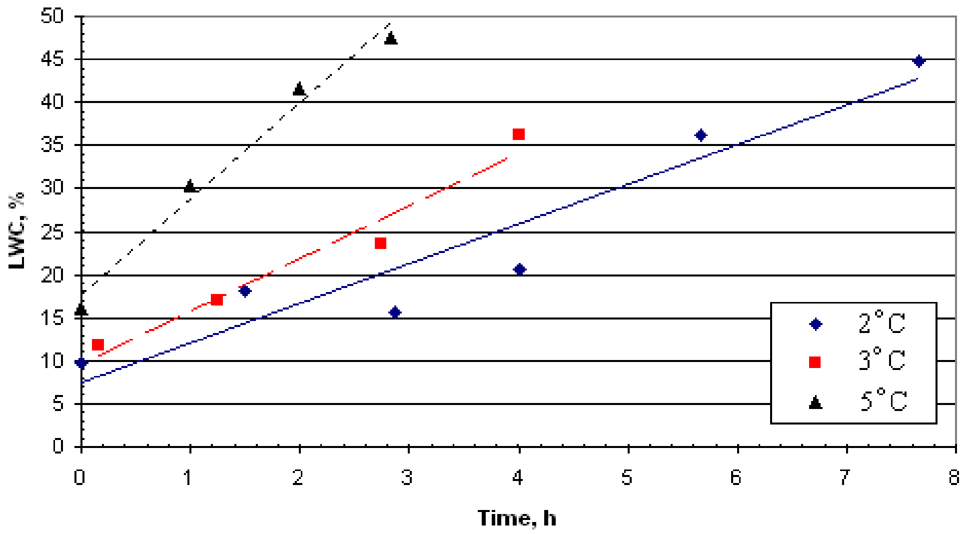

(b)

Fig. 5: Time histories of LWC until snow shedding with air temperature as parameter; (a) $U_a = 4$ m/s, no radiation; (b) $I_r = 900$ lx, no wind

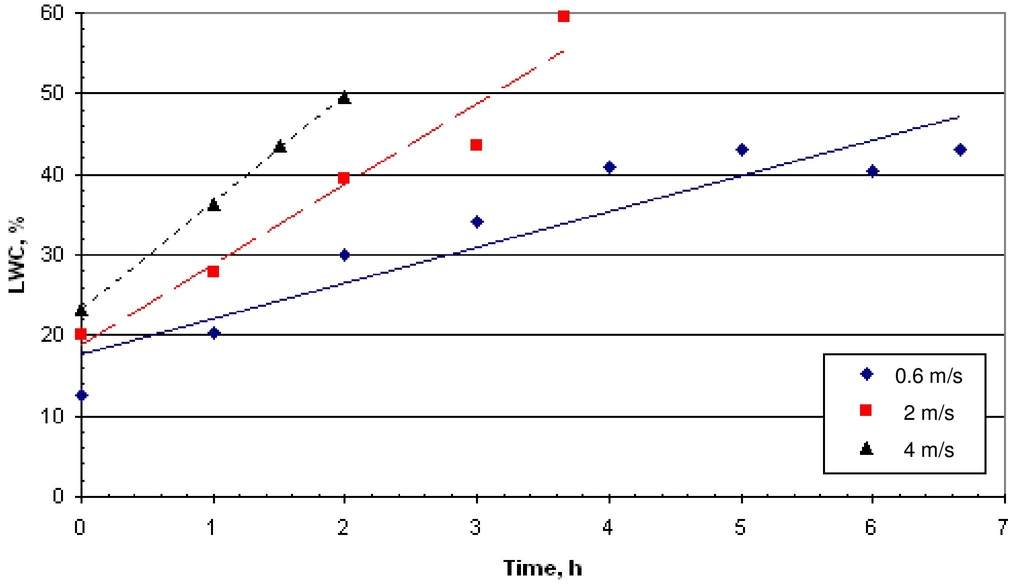

Fig. 6: Time histories of LWC until snow shedding with wind speed as parameter, $T_a = 5\,^{\circ}\mathrm{C}$, no radiation

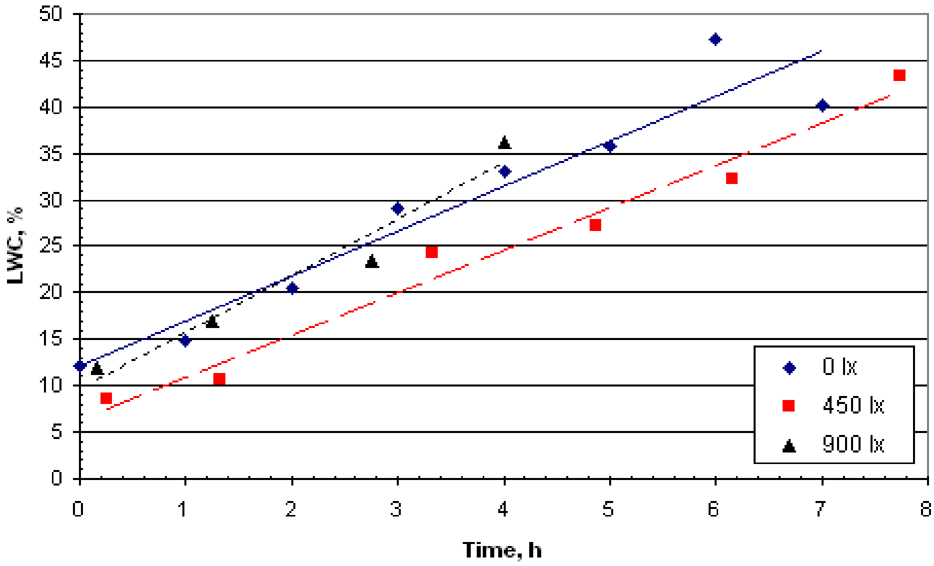

Fig. 7: Time histories of LWC until snow shedding with heat radiation as parameter, $T_a = 3^{\circ}\mathrm{C}$, no wind

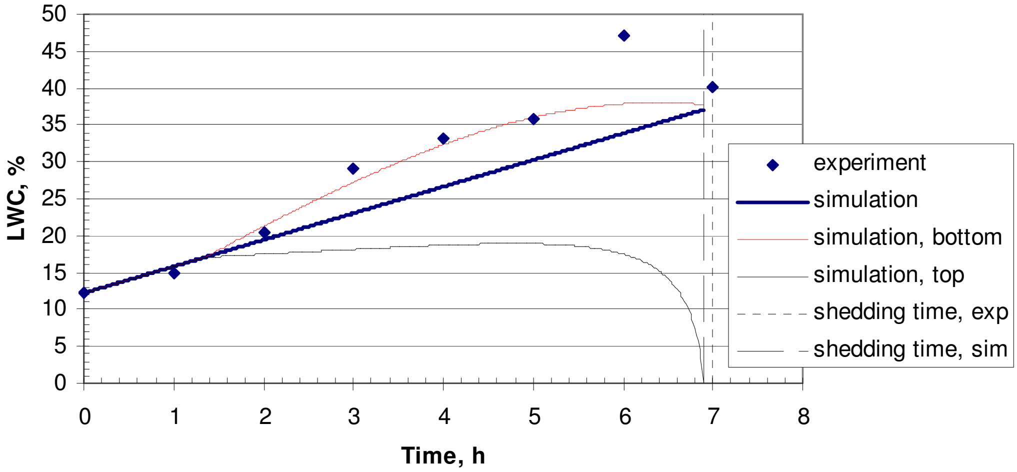
LWC, %
Time, h
experiment
simulation
simulation, bottom
simulation, top
shedding time, exp
shedding time, sim

(a)

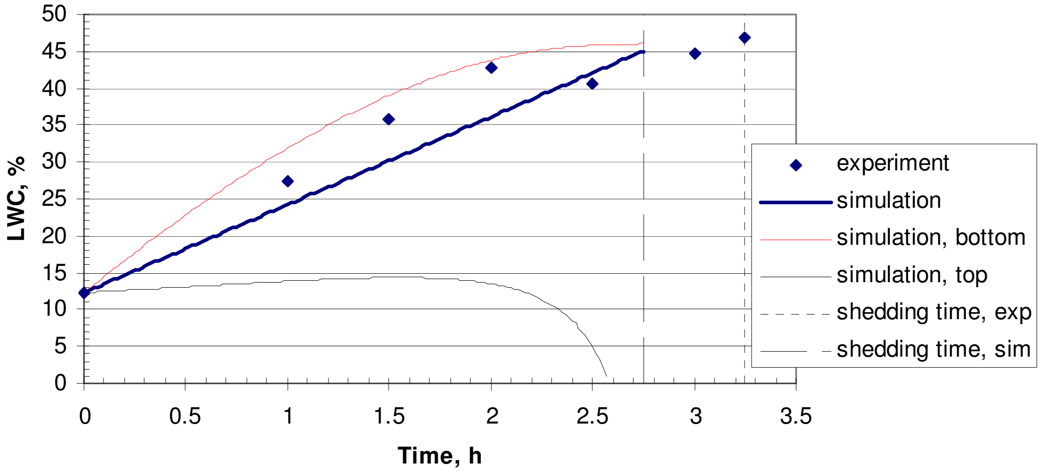
LWC, %
Time, h
experiment
simulation
simulation, bottom
simulation, top
shedding time, exp
shedding time, sim

(b)

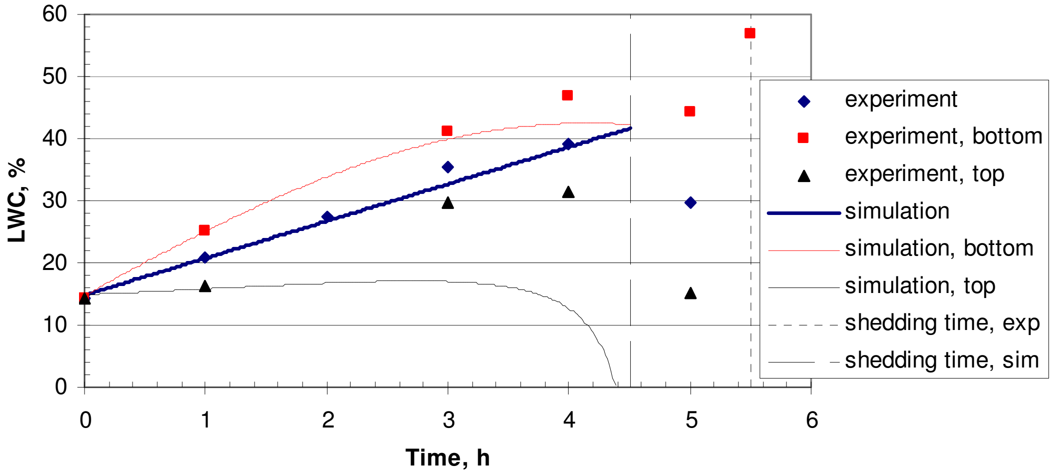

(c)

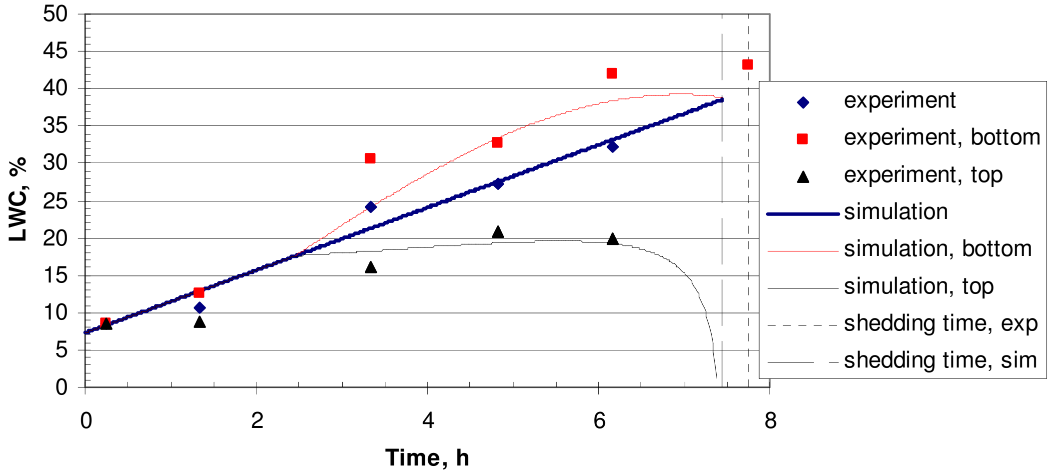

(d)

Fig. 8: Measured (experiment) and calculated (simulation) LWC time histories, (a) $T_a = 3^\circ\mathrm{C}$, no wind, no radiation, (b) $T_a = 3^\circ\mathrm{C}$, $U_a = 4$ m/s, no radiation, (c) $T_a = 2^\circ\mathrm{C}$, $U_a = 4$ m/s, no radiation, (d) $T_a = 3^\circ\mathrm{C}$, no wind, $I_r = 450\,\mathrm{lx}$

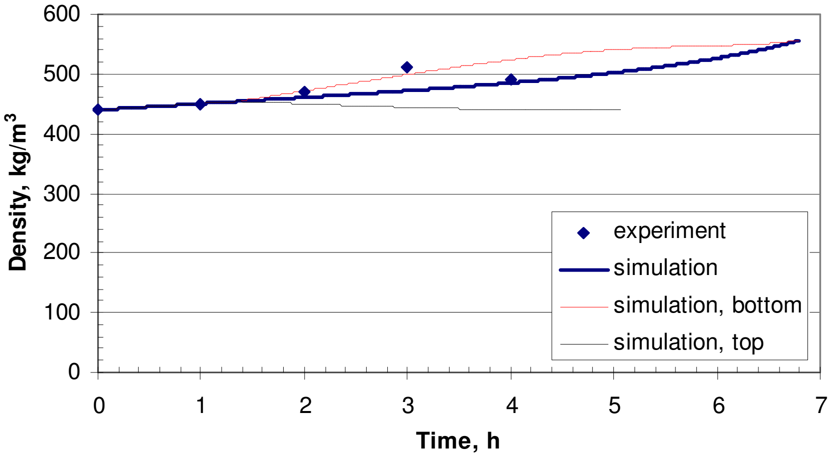

Fig. 9: Measured (experiment) and calculated (simulation) density time histories for $T_a = 3^{\circ}\mathrm{C}$, no wind, no radiation

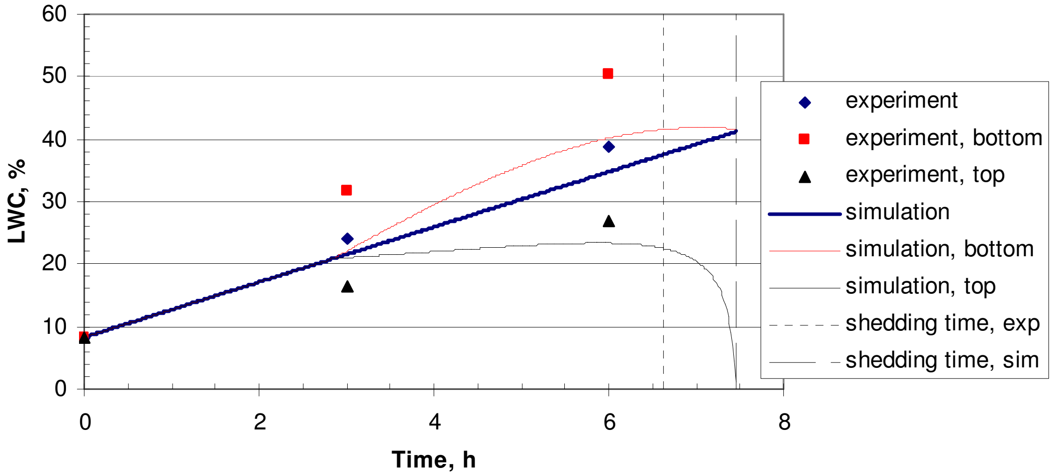

Fig. 10: LWC time histories as measured by Roberge, 2006 (experiment) and calculated by the present model (simulation) for $T_a = 3^\circ\mathrm{C}$, no wind, no radiation